Journal of Materials Science and Engineering with Advanced Technology
Volume 7, Number 1, 2013, Pages 49-73

SYNTHESIZING OPAL-LIKE AND INVERSE OPAL-LIKE STRUCTURES AND THEIR USE AS ELECTRODE MODIFIED SURFACES FOR INDOOR AIR CLEANERS

M. A. AGUAYO SÁNCHEZ[1,2] **and J. J. PÉREZ BUENO**[1]

[1]Centro de Investigación y Desarrollo Tecnológico en Electroquímica
S.C., Parque Tecnológico Querétaro Sanfandila
Pedro Escobedo Querétaro
CP. 76700
México
e-mail: jperez@cideteq.mx

[2]Universidad Autónomo de Zacatecas
Unidad Académica de Ciencias Químicas
Programa de Ingeniería Quimica
Km. 0.5 Carr. a Cd. Cuauhtémoc
Guadalupe, Zacatecas 98600
México
e-mail: chilo_a@hotmail.com

Abstract

Indoor pollution has been studied broadly in recent years due to the issue it represents in public health. This work presents the development of different modified electrodes having opal-like and inverse opal-like structures, to be used as collector plates in an electrostatic precipitator for the deposit of particles suspended in air. Some aspects of the modification of the electrodes in electrostatic precipitators have been analyzed in order to increase the efficiency and capacity for capturing these suspended particles, exchanging the flat plates currently used as collectors for opal-like and inverse opal-like structures. To

Keywords and phrases: electrostatic, precipitator, air, purifying, opal.

Received November 1, 2012; Revised January 8, 2013

© 2013 Scientific Advances Publishers

accomplish this, we studied alternative routes of obtaining these structures. In their preparation, electroless and electrolytic metal deposits were carried onto glass spheres of different sizes, as well as using tin melting for obtaining inverse opals. The best route for preparing opal-like structures of desired sizes was plating of glass beads of 4mm in diameter, while for inverse opals, the most viable way was with tin melting. Also, tests were conducted on electrostatic precipitators with plates of opal-like and inverse opal-like structures, metallic foams and plates. The inverse opal-like structure shows advantages and disadvantages as an electrode for electrostatic precipitators.

1. Introduction

In recent years, pollution problems have become so great and diverse that society has been growing in awareness of current risks and even more, of the potential. As a result of social pressure generated, decision makers show a growing political will to solve the problems. Because of this, it is of great interest in this research area for reducing and, in the present and the future, achieving pollution in the atmosphere at below the permissible limits.

Indoor pollution represents a strategic point in this problem, as in both domestic and industrial use, it is necessary to implement air decontamination systems to reduce the risk of health affectation. Electrostatic precipitators already have increasing use in the removal of biological aerosols in enclosed spaces, such as in hospitals, clinics, the food industry, pharmaceutical facilities, etc.

In order to offer solutions to the problem of suspended particles in indoor air, many different studies have been carried out for the design and optimization of purification systems. Waring et al. in 2008 [22] studied five different portable purifiers, and their efficiencies were determined by examining the deposition rate as a function of particle diameter, with a mean efficiency around 60%. Nevertheless, this was far from the expected efficiency, which was around 90%, mainly attributed to a lack of flow or movement of the air mass within the test chamber. There have been modelling and simulations taking into account many variables involved in electrostatic precipitators [10, 15]: flow, speed, electric forces, kind of particles, and even their sources [2], as well as the relationship between dust density and recollection capacity of plates or electrodes [18].

Also, different types of purifiers have been developed by using photocatalysis in order to additionally precipitate the suspended particles to degrade pollutants. The most commonly used catalyst is titanium dioxide (TiO_2). Kudo et al. [8] succeeded in synthesizing a rectangular column of TiO_2 supported on silica core sheets for later use in the development of an effective air purification system.

Moreover, the arrangement of electrodes in an electrostatic precipitator and the applied voltage are of great importance. Some reports recommended an array of electrodes equal in dimensions, one grounded and applying a voltage to the other, even using nickel propellers [19], while others use two grounded collector plates and a steel wire equidistant to them and perpendicular to the flow, which was connected to a power source applying a voltage of approximately 30kV. These conditions were reported in a study published in 2008 by Podlinski et al. [18] using an acrylic chamber with a volume of $200dm^3$ coupled to other devices in order to evaluate the amount of deposit according to the density of cigarette smoke particles, which were generated from 2 to 14 burning cigarettes and introduced into the flow.

The efficiency of electrostatic precipitators for very fine particles, around one micron in diameter, has been reported as relatively low [14]. Kocik et al. [7] used a setup consisting of an acrylic chamber 1.6m in length with seven steel wires 20cm in length as electrodes and two collector plates at the entrance and at the exit of the duct, with a fan to achieve a desired flow rate. This was performed for different potential values (16-32kV) and at both polarities. The efficiencies were evaluated by using cigarette ashes in the range of 1 - 5μm. After some testing, they came to the following conclusions: It was more efficient at a lower flow, thereby obtaining a higher deposit amount. The behaviour for particles larger than 3μm showed that applying a voltage of 20kV obtained 100% removal. Regarding reverse polarity, no significant change was observed; only at the minimum voltage (16kV) was there a greater removal of

particles smaller than 1μm with positive polarity. The removal of the smaller particles became effective at 25kV, obtaining 100% removal using 32kV.

Modified electrodes have been broadly studied. Kuroda et al. [9] examined the effect of four different aluminum electrodes: One with a smooth surface or mirror finishing and the other three with circular perforations having diameters of 0.6, 1, and 3.1mm in a sandwich arrangement with two glass plates at the ends and a separation of 5.5mm between them. The three electrodes with perforations had higher particle collections than the electrode without modification. The electrode with holes of 3.1mm in diameter had the best performance.

An opal has ordered arrays of spheres of around 0.5μm in diameter, and the space between them can be filled by another material. An inverse opal is obtained by removing the spheres after filling the empty space. Inverse opal structures are currently used in manufacturing photonic crystals. The inverse opals can be synthesized by sol-gel, chemical vapor deposition (CVD), electrolytic and electroless deposition, atomic layer deposition, chemical conversion, etc. For example, the electrochemical technique allows a complete infiltration and fine control in film thickness [23]. Juárez and Lopez [4] reported their growth by zinc electrodeposits into polystyrene spheres by using two different techniques: Cyclic voltammetry and square wave pulsed potential, obtaining an arrangement with smaller pores through the latter but with better homogeneity and order.

Different techniques and materials have been used in preparing photocatalytic TiO_2 inverse opals [12]. The works in this field include doping titania with metals and oxides in order to attain higher absorption in the visible region and avoiding electron-hole recombination [3, 13, 24]. Other photocatalytic material fabricated as inverse opals have ZnO [1, 25], which results in higher areas and illumination capability of regularly opened structures. Also, those structures have been used in photo-electrochemical cells in solar energy harvesting for electricity generation [5, 11].

This work addresses the problem by developing and testing different modified structures and using them as electrodes in electrostatic precipitators. Here, we named the developed structures as opal-like and inverse opal-like due to the difference in pore sizes, since our proposal for air purifiers have millimetric spheres or voids contrasting with sub-micrometric opal and inverse opal structures.

2. Materials and Methods

2.1. Preparing glass/silver opal-like structures

In preparing glass/silver opal-like structures, glass spheres of 3mm and 4mm in diameter were used. A heat treatment of 650°C was applied to the samples for 3.5h in a rectangular steel mold. For the structure surface metallization, a silver finishing was applied through the Brashear formula [16, 17]. This involves wetting a surface with a mixture of two solutions:

(1) Solution A. The first solution consisted of 20g of silver nitrate and 10g of potassium hydroxide in 400mL of distilled water.

The solution had a dark brown precipitate, which was dissolved with ammonium hydroxide and vigorous stirring after each addition. We used around 50mL of this solution.

(2) Solution B. The second solution consisted of 90g of sucrose and 4mL of pure nitric acid in 1L of distilled water. This was heated (90°C) and cooled before use, since an optimum work temperature is 20°C.

The Brashear formula consists of mixing one part of solution B with four parts of solution A (v:v ratio) before use. The opal-like structures were left in contact with this mixture for 16h.

2.2. Preparing glass/nickel opal-like structures

In preparing glass/nickel opal-like structures for use as electrodes, we started with the previously obtained glass/silver opal-like structures and then applied a bright nickel electrodeposit through a nickel sulphamate

based solution with a current of $0.6A/cm^2$ at 60ºC for 1.3h [6, 20]. Finally, those structures were rinsed with distilled water to remove residues of the nickel solution.

2.3. Preparing tin inverse opal-like structures

A pure tin ingot was melted into an electric furnace at a temperature of 400ºC for 3h. Subsequently, the liquid tin was poured within a vessel on dried silica gel beads of an average diameter of 3mm, stirring to allow the tin to pass through the spaces between the particles. This was mostly unsuccessful, since the liquid tin weight displaced the light silica gel beads. Alternatively, silica gel beads were packed in a beaker with a wire mesh on top. A tin ingot was placed on the wire mesh. This arrangement was placed into an electric furnace, and the melted tin passed through the gaps between the spheres. Finally, in order to prepare an inverse opal-like structure, the silica gel beads/tin pieces were chemically treated with a hydrofluoric acid-water solution (1:1, v:v) for 0.5h, which dissolved the inner silica gel beads. This procedure allowed the achieving of results closer to the desired inverse opal-like structure, with an average pore size around 3mm.

2.4. Evaluation of modified electrodes on an electrostatic precipitator

We choose to perform the evaluation of modified electrodes in a commercial electrostatic precipitator having three vertical parallel plates, adapting the structures on plate surfaces. The tests were conducted by using different suspended particles, such as fly ash, talc, methyl orange powder, combustion products of paper, and a silver particle fog achieved with an ultrasonic nebulizer within a glove box. The fly ash is constituted of cenospheres, which originate during coal combustion for electricity generation. They are hollow spheres captured in an industrial electrostatic precipitator, with an average size in the range of 5-10μm. Also, they can be considered as PM_{10} (particles with a size around 10μm), capable of being suspended in aerosols and a potential risk for health.

Figure 1 shows a diagram of a commercial purifier consisting of three vertical parallel plates. The different structures prepared were adapted to such plates in order to conduct the tests. In this design, the plates were anodes, and two wires served as cathodes. The spaces between plates were 2.1cm, as was the distance between the wires. The voltages applied to the plates ranged between 8.5V and 3.1V, whereas in the wires, voltages were from 16.2 to around 19V.

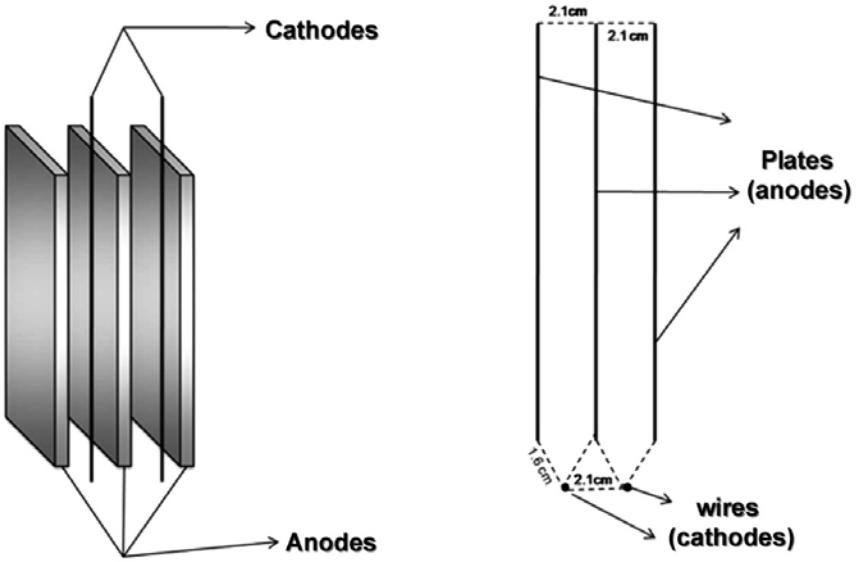

Figure 1. A diagram of the electrostatic precipitator used during the tests.

Figure 2 shows the structures used as electrodes in the electrostatic precipitator: (a) 304 stainless steel plate; (b) a copper coated foam; (c) the obtained metallic opal-like structures coated with silver; (d) nickel; and (e) a tin inverse opal-like structure. The copper coated foam had a total volume around $22cm^3$, an internal empty space volume of approximately $12cm^3$, and a pore spacing around 2mm. The outer exposed area was approximately $40cm^2$.

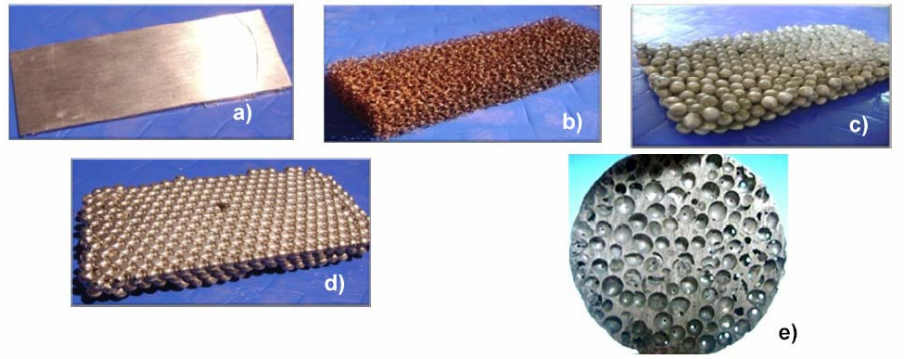

Figure 2. Structures used as electrodes: (a) 304 stainless steel plate; (b) copper coated foam; (c) silver coated opal-like structure; (d) nickel opal-like structure; and (e) tin inverse opal-like structure.

The evaluations of efficiencies of modified electrodes were determined by mass balance in the electrostatic precipitator, considering the known mass of particles used as aerosol, mass adhered to a specific area of a plate, and the amount of mass at the inlet and outlet of the precipitator and taking into account that not all particles were able to enter the precipitator.

In order to evaluate only the space occupied by the structures used as electrodes, the three plates were isolated, leaving only an area of $10cm^2$, adapting each structure on this surface to be studied separately. We used 20g of fly ash for each case.

3. Results and Discussion

3.1. Glass/silver opal-like structures

Glass beads of approximately three millimeters in diameter were used to form opal-like structures. They were placed in a mold and heat treated above 540ºC. This was in order to unite the spheres to each other but without losing their shapes. This was accomplished successfully to the extent of having opal-like structures of various sizes and shapes. For example, a structure was made with a total volume of approximately

24.54cm^3 and internal spaces totaling approximately 4.54cm^3 (a ratio of 5.4:1 between free spaces and bulk glass as determined by the ratio of the total volume of the spheres and the total volume of the structure). The outer exposed area was 53.79cm^2 (Figure 3).

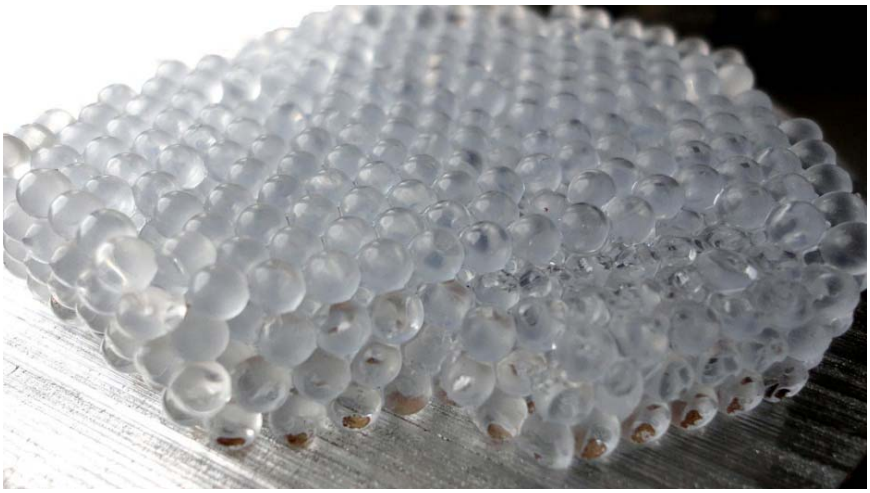

Figure 3. An opal-like structure made with glass beads.

In the case of these structures, a further step was performed with the intention of obtaining conductive surfaces by metallizing them. Using the process with the Brashear formula, the surfaces of spheres in opal-like structure were metallized. An opal-like structure of spheres having 1mm in diameter remained less time in the plating solution and obtained a lighter color, but showed the lowest electrical resistivity in all parts coated with silver.

After this, in order to obtain a structure with a geometry that could be coupled to the electrostatic precipitator for evaluation, a steel mold was used having a volume of 75cm^3, obtaining an arrangement 5cm wide, 9.5cm long, and 1.1cm high. Figure 2(c) shows such structure coated with a silver solution. The foreground of the structure consisted of 25 spheres in length and 12 spheres wide, which represented an approximate surface area of 144.82cm^2, considering spheres having

3.92mm in diameter. This was also considering that voids are immediately below the top of spheres in a second layer, which offset and covered the empty spaces.

3.2. Glass/nickel opal-like structures

As a final step of the process, and with the aim of achieving a homogeneous conductor surface with good adhesion and mechanical resistance, electrodeposition was carried out from a nickel sulphamate bath. An opal-type metal structure with a deposit of Ni was obtained that presented good characteristics for subsequent use as an electrode in an electrostatic precipitator. The opal glass-Ni metal is shown in Figure 4 (or Figure 7(d).

Figure 4. A glass/nickel opal-like structure.

The thickness of Ni deposition was determined by measuring cross-sectional thickness by ASTM B487-85 (07), obtaining an average of 24.16 microns with a standard deviation of 1.10μm. Measurements of the samples are presented in Table 1.

Table 1. Thickness measurements of electrolytic nickel

Sample	Thickness (μm)
1	21.71
2	24.22
3	23.34
4	24.74
5	24.35
6	25.45
7	24.31
8	24.39
9	25.06
10	25.01

One of the observations noted in samples obtained by the procedure used involved the center of such coated structures, which showed a different color from that of silver and bright nickel. This began from the third row of spheres inwards and the second row starting from the bottom, as seen in Figure 5. This was attributed to a blockage of the current density required for nickel deposition and to the presence of sulphur. The apparent tone was originally a light pearl-like color, with a slightly yellow tint and a metallic gray finish, only observed in specular reflection, attributable to a thin nickel coating. The color turned to yellow after aging. The relevance of this deposit was due to both an aesthetic appearance of the spheres and the presence of silver-sulphur (from the nickel sulphamate bath) and a thin coating of nickel. Presumably, this effect resulted from the use of the nickel sulphamate solution after silver plating in conjunction with blocking the field lines inside the structure, forming a sulphur layer but without forming Ag_2S, as in the case of patina formation on silver surfaces by reaction with hydrogen sulphide (H_2S), which has a black tone.

Figure 5. Yellow spheres in the inner part of opal-like glass structures coated with Ag/S/Ni.

Figure 6 shows the diffractogram corresponding to those yellow spheres. The main crystalline structure was silver (JCPS 65-2871). There were sulphur and other compounds present with nickel, such as NiS and Ni_3S_4 (not shown in Figure 6 for clarity). The crystalline Ag_2S structures were not detected. Also, metallic nickel was not detected on those yellow spheres.

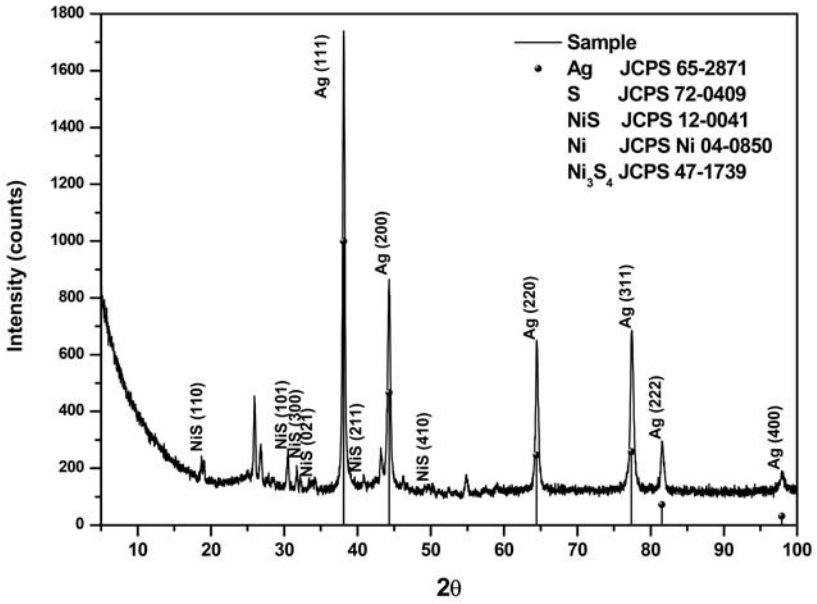

Figure 6. Diffractogram of yellow spheres shown in Figure 5.

Figure 7 show reflectance and absorbance spectra corresponding to opal-like structures coated with Ag-Ni (inner areas) and Ni (outer areas) and an opal-like structure coated with silver by using the Brashear formula for comparison. This was done in order to compare the obtained coating on the central part of the structure (Figure 5). The spectrometer (Ocean Optics USB2000) had an integrating sphere with an aperture of 8mm in diameter. The spectra show a quasi-linear behaviour in the visible region, with characteristic slopes for each metal.

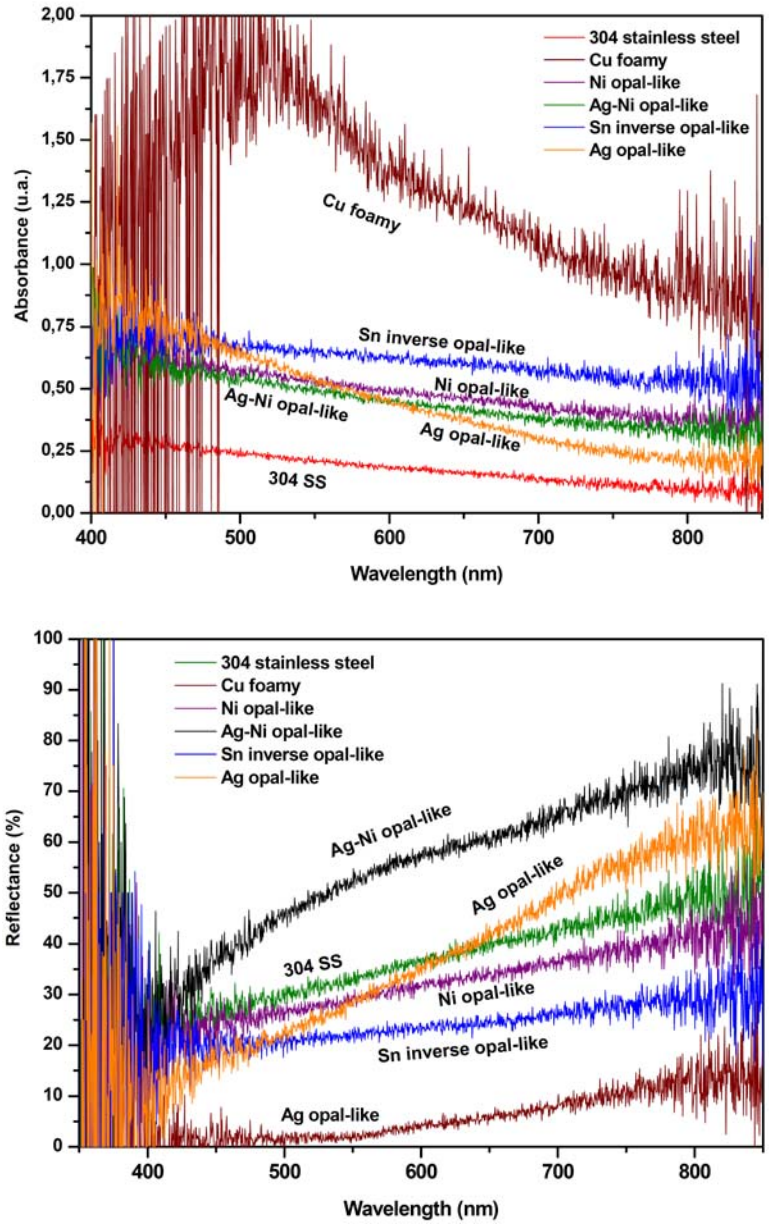

Figure 7. Absorbance and reflectance spectra corresponding to opal-like structures with Ag-Ni, Ag, and Ni metallized surfaces. Cu foam, stainless steel plate, and inverse opal-like structure are also shown.

The transmittance was not equal to zero in the case of the measurements conducted on open or porous structures, either by direct transmission through the sample or diffuse scattering structure their tunnels. The Cu foam shows a high transmittance, which directly affects the absorbance and reflectance measurements. Other structures also had light loss at the surface voids. There were differences among the opal-like structure coated with Ag by the Brashear formula and the other corresponding to the central part of the nickel opal-like structure, allowing us to identify that it is not just silver. Complementarily, the reflectance spectra show a reverse order, with a higher reflectance of opal-like Ag-Ni, Ag, and Ni. Table 2 shows parameters of color for these opal-like structures. The CIE L^* parameter shows the nickel structure as a very dark 38.4 (in a range 0-100). All samples have dominant wavelength around 590nm. The nickel had relatively low color purity. Moreover, silver structures differ basically in the *x* coordinate, allowing us to identify a slight difference in color of both coatings.

Table 2. Color parameters corresponding to opal-like structures coated with Ag, Ag-Ni, and Ni

Color parameters	Ag opal	Ag-Ni opal	Ni opal
X	0.4883	0.5014	0.4725
Y	0.4177	0.4157	0.1186
CIE L^*	61.9	63	38.4
CIE a^*	7	10.8	4
CIE b^*	19	23.9	6.2
Dominant wavelength (nm)	587	585.4	593.5
Color purity	0.354	0.43	0.183

Figure 8(a) shows the observation by electron scanning microscopy (SEM) at a 1500× magnification, which allows us to see the topography of a Ag coated sphere corresponding to the internal part of the structure of Figure 7. There was a continuous surface, mainly composed of aggregated particles of a few microns. An EDS (energy dispersive X-ray spectroscopy) micro-analysis identified the presence of silver, nickel, and sulphur. Figure 8(b) presents the graph of composition values on a point analysis. This may be relevant due to the presence of sulphur in silver while preserving an excellent surface aesthetic quality, which may result in a stable surface for ornamental practical purposes. Aside from the characteristics that may be relevant to other applications, there is not a direct impact of the Ag-Ni coating, since it was electrically conductive and occurs in the third layer of spheres, which does not have a significant contribution to the uptake arrangement of particle deposition in the described setup.

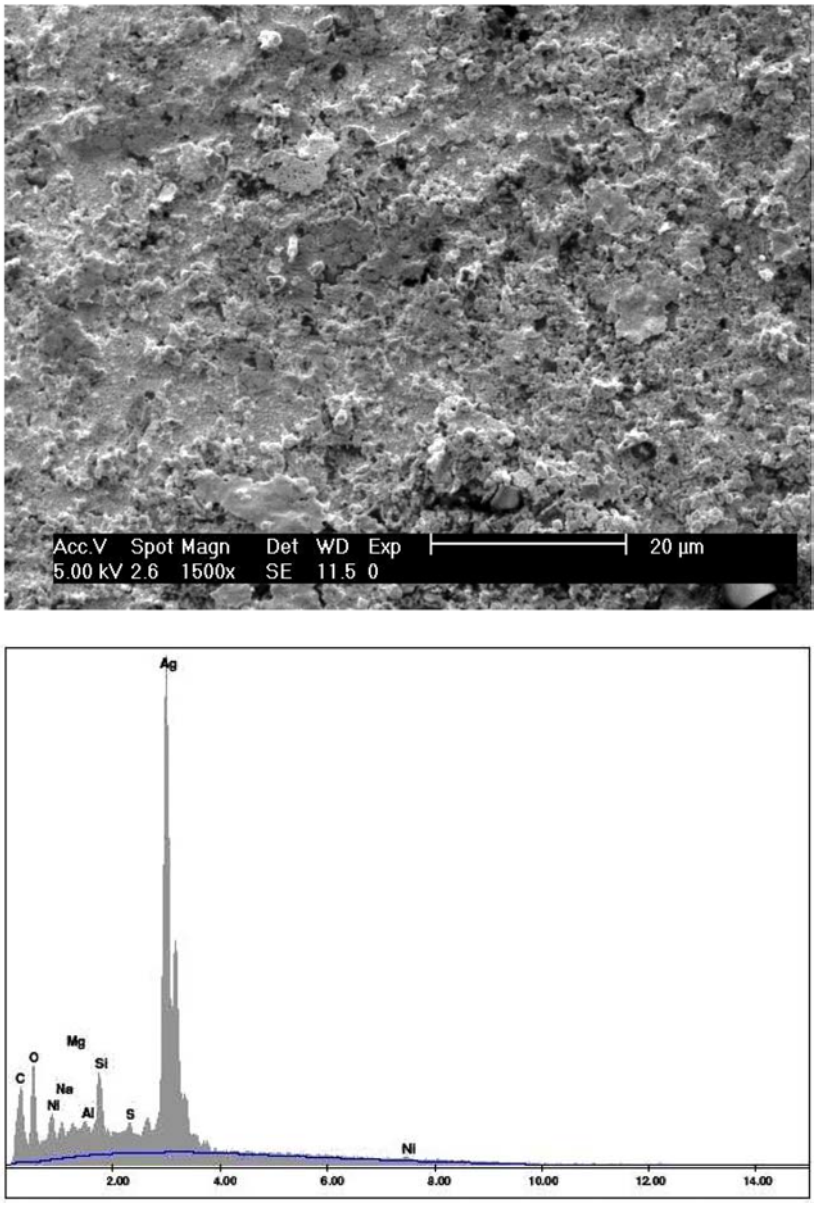

Figure 8. (a) Micrograph of the surface of a sphere with nickel-silver finishing corresponding to the central section of the structure in Figure 7; (b) the corresponding EDS spectrum.

Other structures were prepared in order to prevent low current density, as in the structure described above, and for obtaining a bright nickel deposit in the inner layers in a similar form as for the silver-glass electrode. A rectangular mold was used with only three glass bead layers of spheres 4mm in diameter. This was also done in order to adapt the geometry to the electrode plate and make a calculus of the effective area exposed (Figure 2(d)). The surface areas were determined for the whole arrangement by using the following equation:

$$A = (\pi L_1 L_2 L_3) / (2r), \tag{1}$$

where L_i was the structure lateral length and r the sphere radius.

3.3. Tin inverse opal-like structures

After chemical treatment with hydrofluoric acid solution, the silica gel spheres were removed, obtaining the inverse opal-like structure. Figure 9 shows the structure of tin with pores around 3mm in diameter and interconnecting tunnels of less than 1mm in diameter.

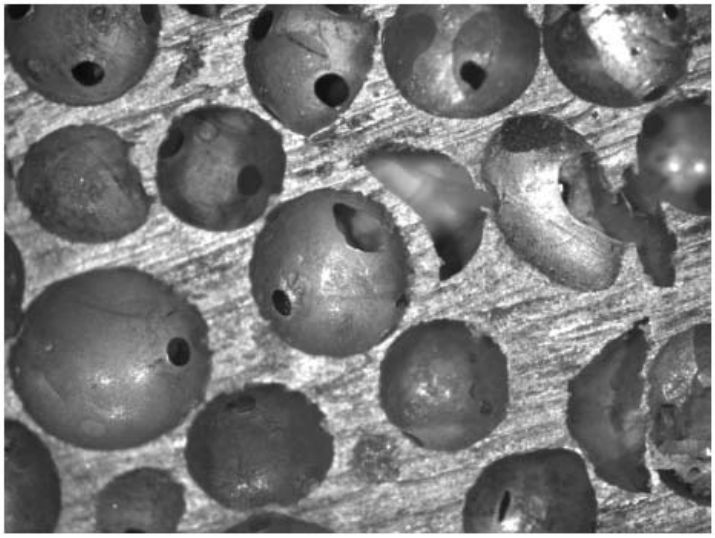

Figure 9. Inverse opal-like structure made with tin.

3.4. Evaluation of modified electrodes on an electrostatic precipitator

The measurement of electrostatically deposited particles of fly ash and methyl orange showed almost the same behaviour (Figures 10 and 11).

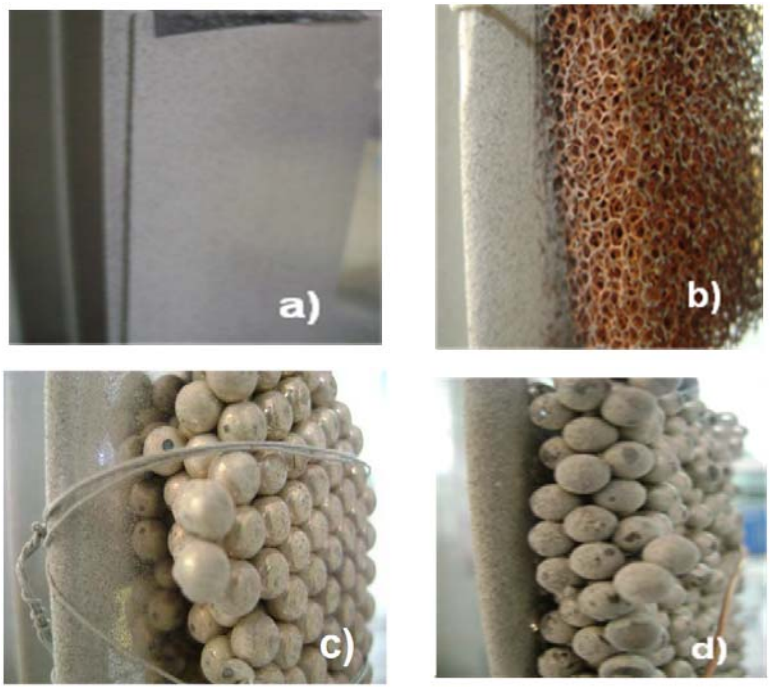

Figure 10. Deposition of fly ash cenospheres onto a: (a) plate with mirror finishing; (b) copper coated foam; (c) silver coated opal-like structure; and (d) nickel coated opal-like structure.

In both cases, using fly ash and methyl orange, particles showed homogeneous deposition onto the tested surfaces, which were completely covered as shown in Figures 10(a) and 11(a). In those figures, the close-ups were taken on the side, where the cathode wires were located, and those surfaces had a thick deposited layer. The deposition on the sponge depends on its pore size, allowing the flow of particles through. Another important factor was the current density from point to point in the mesh, with higher deposits at points closer to the current supplier.

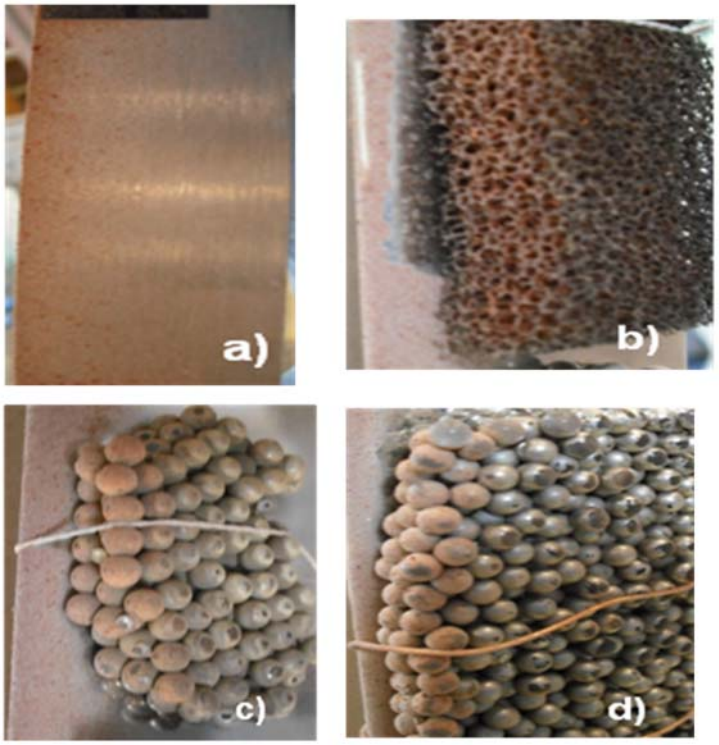

Figure 11. Deposition of methyl orange particles onto a: (a) plate with mirror finishing; (b) copper coated foam; (c) silver coated opal-like structure; and (d) nickel coated opal-like structure.

Regarding the opal-like structure, the difference was due to the current density at the surface. In the case of the silver-like structure, the silver tarnish form a chemical reaction with atmospheric sulphur on its surface (starting a patina layer) decreased the conductivity, showing some differences with the opal-like structure coated with nickel. Comparing with the commercial purifier, the arrangement had resistance to the flow of particles, so that there was an increased deposition in the foreground reaching the saturation point. This means that the structure pore sizes were not enough for an optimum flow. However, the arrangement of spheres in opal configuration presents a larger area in the foreground. This can be appreciated in the micrographs of Figure 12, which show the deposits within the pores of inverse opal-like structures.

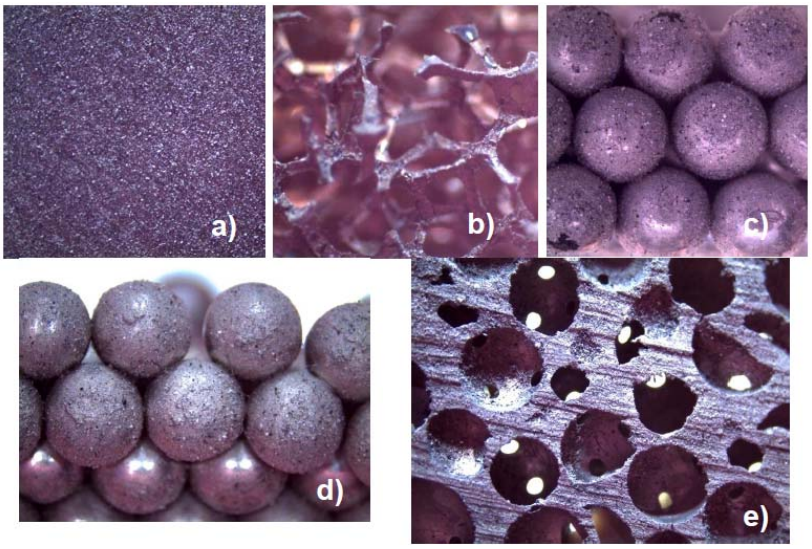

Figure 12. SEM micrograph of fly ash deposits onto a: (a) plate with mirror finishing; (b) copper coated foam; (c) silver coated opal-like structure; (d) nickel coated opal-like structure; and (e) tin inverse opal-like structure.

A combination of both favourable characteristics of the mesh and opal-like structures occurs in the inverse opal-like structure. This structure consists of solid material in the original spaces between the glass beads and opal-like voids in their sites. This structure allows the aerosol particles to flow through its channels, which can be designed to achieve an optimum balance between flow resistance and surface area. In order to calculate the inverse opal-like structure effective area, a modification to Equation (1) was proposed. Equation (2) considers the reduction of area due to the channels between spherical voids

$$A = (\pi L_1 L_2 L_3) / (2r) - 6\pi(r_{\text{tun}})^2, \quad (2)$$

where r_{tun} is the radius of a cross-sectional area of the tunnel or channel, L_i is the length of the array side, and r is the sphere radius. The r_{tun} can be adjusted to have an optimum flow through this structure.

Table 3 shows the areas of the electrodes for comparison. Assuming that a tin inverse opal-like structure with the desired characteristics was obtained and comparing with a reference plate with mirror finish having an area of $46\,cm^2$, the prepared opal-like and inverse opal-like structures had an area increase up to 300% for the first layer of spheres. The inverse opal-like structure had a slightly lower area, due to the tunnel connections. However, this had a lower resistance to flow than the opal-like structure, allowing a higher deposition of particles. Thus, this structure provides an optimization in the use of space within the precipitator.

Table 3. Computed areas and efficiencies for the electrodes

Electrode	Area (cm^2)	% dust retention
Steel plate (mirror finishing)	46	80.7
Glass/silver opal-like structure	144.82	92.3
Glass/nickel opal-like structure	144.82	94.29
Tin inverse opal-like structure	144.78	89.2

However, regardless of the area difference between opal-like and inverse opal-like structures, the manufacturing process for the former was slow, which included depositing different coatings. The inverse opal-like structure was easier, faster, cheaper, and recyclable, but obtaining perfect structures was more complicated.

Table 3 shows the computed electrode efficiencies, which shows that the best particle retention was obtained by the nickel opal-like structure. This had higher uniformity and conductivity, compared to the silver one, despite having the same areas.

The inverse opal-like structure was expected to have better results. However, it was difficult to obtain and adjust a symmetric and tunneled structure having a crystal-like structure with higher transmission in the three axes. One factor influencing the distribution of the deposits on the electrodes was the relationship between the wire distance to the collector plate and the applied voltage, i.e., the electric field intensity.

4. Conclusion

Metallic opal-like structures were obtained both with nickel and silver, as well as an inverse opal-like structure made with tin. The best way tested of obtaining opal was by coating an opal-like structure made with glass beads, 4mm in diameter, previously stuck together by heat treatment. A coating of silver was applied to them by Brashear's formula and a subsequent nickel electrodeposition. For an inverse opal-like structure, the assayed technique, which allowed obtaining it in a desired size was by melting tin over silica gel beads and removing them with a dilute aqueous solution of hydrofluoric acid, thereby obtaining a structure having pores of 3mm with a connecting tunnel diameter up to 1mm.

These structures provide a greater surface area compared to that of an electrode with mirror finishing or flat surface, increasing it by up to 300% for the obtained structures. This can optimize inner surfaces of an electrostatic precipitator, allowing an increment of the ability to capture suspended particles. Nevertheless, their cleaning can be achieved not by contact, but by washing or by outdoor air blowing.

The analyzed structures, both the mesh and opal, presented favourable and unfavourable factors. In the case of the mesh, its open structure offers less resistance to flow of the particles but low current distribution. Furthermore, the opal has a larger surface area but greater flow resistance.

Deposition of particles had similar thicknesses and uniformity of deposition for the different analyzed structures in an electrostatic precipitator assembly. Their capacities were directly related to the effective area and the distance among the cathode wire and the surfaces of the anode and were inversely proportional to the flow resistance.

The metallic inverse opal-like structure combines both factors, increment of the capacity and deposition efficiency of the suspended particles, as well as improved mechanical strength compared to opal-like structures made of glass beads. However, an improvement of the arrangement and distances between cathodes and anodes of the precipitator may also improve, in part, the available area for flat surfaces.

The work offers a glimpse of an inverse opal-like structure capability of increasing the area of anodes closer to the cathode and that it could combine both increments of capacity and efficiency of deposition of suspended particles.

Acknowledgement

The authors gratefully acknowledge the financial support from the Mexican Council for Science and Technology (CONACyT, Grant CB-2009-01 133157). Also, the first author acknowledges CONACyT for her graduate fellowship. The authors are especially grateful to Darlene Garey of the US Peace Corps for her valuable suggestions for this work.

References

[1] V. Abramova and A. Sinitskii, Large-scale ZnO inverse opal films fabricated by a sol-gel technique, Superlattices and Microstructures 45 (2009), 624-629.

[2] J. Chang, Journal of Electrostatics 57 (2003), 273-291.

[3] Y. Jin, Y. Zhu, X. Yang, Ch. Wei and Ch. Li, Fabrication and characterization of cerium-doped titania inverse opal by sol-gel method, Materials Chemistry and Physics 106 (2007), 209-214.

[4] B. H. Juárez and C. López, J. Phys. Chem. B 108(43) (2004), 16708-16712.

[5] S. K. Karuturi, Ch. Cheng, L. Liu, L. T. Su, H. J. Fan and A. I. Y. Tok, Inverse opals coupled with nanowires as photo-electrochemical anode, Nano Energy 1 (2012), 322-327.

[6] J. J. Kelly, S. H. Goods, A. A. Talin and J. T. Hachman, Electrodeposition of Ni from low-temperature sulfamate electrolytes I, Electrochemistry and film stress, Journal of the Electrochemical Society 153 (2006), C318-C324.

[7] M. Kocik, J. Dekowski and J. Mizeraczyka, Journal of Electrostatics 63 (2005), 761-766.

[8] T. Kudo, Y. Kudo and A. Ruike, Catalysis Today 122 (2007), 14-19.

[9] Y. Kuroda and Y. Kawada, Journal of Electrostatics 57 (2003), 407-415.

[10] H. Lei, L. Wang and Z. Wu, Journal of Computational Physics 193 (2004), 697-707.

[11] L. Liu, S. K. Karuturi, L. T. Su and A. I. Y. Tok, TiO_2 inverse-opal electrode fabricated by atomic layer deposition for dye-sensitized solar cell applications, Energy Environ. Sci. 4 (2011), 209-215.

[12] L. Liu, S. K. Karuturi, L. T. Su, Q. Wang and A. I. Yoong Tok, Electrochromic photonic crystal displays with versatile color tenability, Electrochemistry Communications 13 (2011), 1163-1165.

[13] Y. Ma, J. F. Chen, Y. Ren and X. Tao, Transition metal-doped titania inverse opals: Fabrication and characterization, Colloids and Surfaces A: Physicochem. Eng. Aspects 370 (2010), 129-135.

[14] A. Mizuno, IEEE Trans. Dielectr. Electr. Ins. 5 (2000), 615-624.

[15] K. S. P. Nikas, A. A. Varonos and G. C. Bergeles, Journal of Electrostatics 63 (2005), 423-443.

[16] Patent US3372059-A, Dow Chem GMBH; Ag, Cu or Ni-plating onto non-conductive glass or plastic surfaces by the Brashear, Rochelle salt or formaldehyde wet reduction processes is improved by the add, 1968.

[17] Patent US4403001; Grenier; John W. (General Electric Company), Electroless application of a silver coating to diamond particles, 1981.

[18] J. Podlinski, A. Niewulisa, J. Mizeraczyka and P. Attenc, Journal of Electrostatics 66 (2008), 246-253.

[19] M. Sillanpää, M. Geller, H. Phuleria and C. Sioutas, Journal of Aerosol Science 39 (2008), 335-347.

[20] Y. Tsuru, M. Nomura and F. R. Foulkes, Effects of boric acid on hydrogen evolution and internal stress in films deposited from a nickel sulfamate bath, Journal of Applied Electrochemistry 32 (2002), 629-634.

[21] A. Wang, S. L. Chen, Peng Dong and Z. Zhou, Preparation of photonic crystal heterostructures composed of two TiO_2 inverse opal films with different filling factors, Synthetic Metals 161 (2011), 504-507.

[22] M. S. Waring, J. A. Siegel and R. L. Corsi, Ultrafine particle removal and generation by portable air cleaners, Atmospheric Environment 42(20) (2008), 5003-5014.

[23] S. H. Yeo, L. K. Teh and C. C. Wong, J. Porous Mater. 13 (2006), 281-285.

[24] Y. Zhao, B. Yang, J. Xu, Z. Fu, M. Wu and F. Li, Facile synthesis of Ag nanoparticles supported on TiO_2 inverse opal with enhanced visible-light photocatalytic activity, Thin Solid Films 520 (2012), 3515-3522.

[25] Y. Zhang, M. Fu, J. Wang, D. He and Y. Wang, Photonic crystal heterostructures fabricated by TiO_2 and ZnO inverse opals using colloidal crystal template with single kind of microspheres, Optical Materials 34 (2012), 1758-1761.

■